

Assessment of continuous sky view factor based on ultra-high resolution natural colour images acquired by remotely piloted airborne systems for applications in an urban area of Athens

Panagiotis T. Nastos , Emmanuel Vassilakis , Marina-Panagiota P. Nastos , Ioannis Charalampopoulos & Andreas Matzarakis

To cite this article: Panagiotis T. Nastos , Emmanuel Vassilakis , Marina-Panagiota P. Nastos , Ioannis Charalampopoulos & Andreas Matzarakis (2017) Assessment of continuous sky view factor based on ultra-high resolution natural colour images acquired by remotely piloted airborne systems for applications in an urban area of Athens, International Journal of Remote Sensing, 38:20, 5814-5829

To link to this article: <http://dx.doi.org/10.1080/01431161.2017.1346845>



Published online: 06 Jul 2017.



Submit your article to this journal [↗](#)




View related articles [↗](#)



View Crossmark data [↗](#)



Assessment of continuous sky view factor based on ultra-high resolution natural colour images acquired by remotely piloted airborne systems for applications in an urban area of Athens

Panagiotis T. Nastos^a, Emmanuel Vassilakis ^a, Marina-Panagiota P. Nastos^b, Ioannis Charalampopoulos^c and Andreas Matzarakis^d

^aDepartment of Geology and Geoenvironment, National & Kapodistrian University of Athens, Athens, Greece; ^bSchool of Architecture, National Technical University of Athens, Athens, Greece; ^cLaboratory of General and Agricultural Meteorology, Agricultural University of Athens, Athens, Greece; ^dResearch Center Human Biometeorology, German Meteorological Service, Freiburg, Germany

ABSTRACT

The thermal comfort conditions in a complex urban area is influenced by the surrounding structures and obstacles which modify the incoming radiation fluxes. A measure of this modification is the sky view factor (SVF), which could be estimated in each point of a selected area if a high resolution digital elevation model (DEM), or other urban morphological data including the manmade infrastructure, are available. The goal of this study is to model the continuous SVF for a complex building environment in the campus of National and Kapodistrian University of Athens, based on a high resolution DEM (0.09 m). For this purpose, we applied the structure-from-motion (SfM) technique, which takes advantage of the interpretation of ultra-high resolution colour images acquired by remotely piloted airborne systems, also known as drones or unmanned aerial vehicles. A quantitative analysis, by applying statistical metrics, yields perfect agreement between modelled and observed SVF values, over the examined area. The proposed methodology could be applied for human-biometeorology research in micro scale complex urban environments.

ARTICLE HISTORY

Received 30 September 2016
Accepted 19 June 2017

1. Introduction

The urbanization phenomenon, referring to the increasing number of people that live in urban areas, is not a modern phenomenon resulting in the physical growth of urban areas, either horizontal or vertical. According to the United Nations Department of Economic and Social Affairs (2014), the urban population of the world has grown rapidly from 746 million in 1950 to 3.9 billion in 2014. The world's population living in urban areas is projected to increase from 54% in 2015 to 60% in 2030 and to 66% by 2050. As a consequence, the development of cities establishes the urban heat island (UHI) effect, which is defined as the rise in ambient temperature in a city or metropolitan area

CONTACT Panagiotis T. Nastos  pnastos@geol.uoa.gr  Department of Geology and Geoenvironment, National & Kapodistrian University of Athens, Athens 15784, Greece

© 2017 Informa UK Limited, trading as Taylor & Francis Group

against its nearby rural areas due to human activities. The open land and the vegetation have been replaced by buildings and roads, which are releasing huge quantities of heat (Nastos and Kapsomenakis 2015). Moreover, the UHI effect, the contribution of which in large scale warming trends is quite small (Jones, Lister, and Li 2008; Kondratyev and Varotsos 1995), influences not only the humans and the cities but also the ecosystems, which are located away from the city centre (Nastos and Kapsomenakis 2015).

Urbanization also led to the need for better urban planning in order to improve the thermal environmental conditions especially in outdoors spaces. The human thermal perception in urban areas is directly influenced by ambient parameters, such as air temperature, humidity, solar radiation, and wind speed (Nikolopoulou, Baker, and Steemers 2001; Svensson and Eliasson 2002; Shashua-Bar and Hoffman 2003; Matzarakis, Rutz, and Mayer 2010; Lin et al. 2013). These variables are modified by the complex micro-environments appeared within the urban structure, taking extreme values in specific cases. The urban canyon geometry in terms of orientation (N–S; E–W), sky view factors (SVF) and/or height:width ($H:W$) ratios have been used in both observational and modelling studies to develop relations with energy and heat exchanges (Grimmond et al. 2001; Charalampopoulos et al. 2013; Jamei et al. 2015). The SVF plays a significant role to determine the incoming radiation fluxes in a complex urban environment (Oke 1981; Oke et al. 1991; Holmer, Postgård, and Eriksson 2001; Nunez, Eliasson, and Lindgren 2000). It is a dimensionless measure between zero and one, representing totally obstructed and free spaces, respectively (Oke 1988). The first yet brief definition for the sky view factor is provided by Watson and Johnson (1987) and is described as ‘SVF is the ratio of incoming radiation received by a planar surface from the sky to that received from the entire hemispheric radiating environment’. This definition is accepted and preferred by academic community (e.g. Brown, Grimmond, and Ratti 2001; Lindberg and Grimmond 2010; Wu, Zhang, and Meng. 2013; Gál, Lindberg, and Unger 2009).

SVF referred also as planar or spheric SVF in biometeorological studies, which focus on the quantification of human thermal environmental conditions. The differences between the planar and the spheric SVF is that the planar type can be expressed as the radiation coming from the visible part of the sky divided by the total radiation from the entire hemisphere (Mandanici, Conte, and Girelli 2016) when the spheric one defined the SVF as the portion of visible sky in the entire celestial hemisphere centred on the observation point (Zakšek, Oštir, and Kokalj 2011). According to Mandanici, Conte, and Girelli (2016), the first definition comes from the concept of the view factor and accounts for the projection of each element of the observed surface in the plane of the observing surface. Instead, the second definition expresses SVF as the proportion of the sky that is visible from a point to the overall sky dome. With this last meaning, the parameter is also called sky-exposure. The planar SVF can give a more radiation-wise approach when spheric one introduces a more geometric approach. The geometric information can be a solid basis for high accuracy estimations of micrometeorological and biometeorological parameters. Thus, the following analysis refers only to the SVF spheric, as it is used more in biometeorological studies. In this point, we have to mention that spheric and planar SVF calculations are based on the fundamental definition of Watson and Johnson (1987).

The modelling of the continuous SVF in each point of a specific area requires a high resolution digital elevation model (DEM) or other urban morphological data including the manmade infrastructure. There are different techniques that estimate the continuous SVF,

such as an extension to ArcView GIS (Souza, Rodrigues, and Mendes 2003; Gál, Lindberg, and Unger 2009), the Solweig model (Lindberg, Thorsson, and Holmer 2008) and the SkyHelios model (Matzarakis and Matuschek 2011) (see more details in Section 2).

The last few years quite a few techniques have been developed aiming to produce a fine and accurate representation of the earth's surface including any manmade infrastructure above it. The main objective was to translate the morphology in digital format with the least loss of detail. Therefore, different kinds of equipment were used in order to achieve satisfying results. Initially classic photogrammetric techniques were used for the interpretation of aerial photographs. The results were quite satisfactory but the achieved resolution as well as the accuracy was rather insufficient for high detail projects. A different perspective for accomplishing the goal of producing a higher resolution surface model was given by airborne laser scanning (lidar). The lidar technology equipment uses the laser light to measure the distance between the laser scanner and the illuminated object and the measurement is independent of external illumination by sunlight (Gallay 2012). This technique is currently replacing the classic photogrammetry in creating DEMs as it is proved to be more detailed and accurate method. One of the major advantages of lidar data interpretation refers to the ability of reconstructing the land surface by 'removing' the vegetation canopy and consequently producing more accurate DEMs even in densely forested areas (Kraus and Pfeifer 1998).

The advancing technology in computer science and digital image analysis and interpretation have led to the development of a novel photogrammetric approach called structure-from-motion (SfM), which offers a fully automated methodology capable of producing high resolution DEMs with low cost equipment (Fonstad et al. 2013; Javernick, Brasington, and Caruso 2014). The generated high-resolution topography and the co-registered final ortho-image is produced by an unstructured set of overlapping photographs taken from varying viewpoints, by remotely piloted airborne systems (RPASs), also known as drones or unmanned aerial vehicles (UAVs). Furthermore, the flexibility, comparative low cost and ease of UAVs deployment overcomes many of the limitations of the temporal 'snapshot' provided by manned aircraft. Besides UAVs could be used to construct atmospheric profiles against traditional high cost infrastructure such as balloons, radiosondes and tall towers (Dumas and Baker 2016). This technique decreases significant cost, time, and logistical limitations of lidar technique and other topographic surveying methods (Johnson et al. 2014). The development and wide usage of the UAVs not only gives a push to techniques, such as the 'SfM' but provides new promises with respect to atmospheric research. UAVs can be used in measuring profiles of the air temperature and humidity in the lowest levels of Earth's atmosphere, remote scale of small-scale surface features, performing storm damage assessment, measuring wind and turbulence in the lowest level of the boundary level. Furthermore, they are ideal to map the thermal land surface temperature with infrared cameras linking the dynamics of a developing boundary layer to observed changes in the heat and water fluxes at the land surface. The production of a fine detailed DEM which includes the human intervention on the earth topography is a significant requirement for the completion of the methodology discussed in this study. The goal of this study is to demonstrate a methodology based on high resolution colour images acquired by low cost RPAS, in order to construct a high-resolution DEM, which is identical for the modelling of the continuous SVF for each point of the examined complex area, contributing in biometeorological studies in micro urban environments.

2. Data and methodology

The study area concerns the complex building environment along with the open areas of the Departments of Physics and Mathematics within the campus of National and Kapodistrian University of Athens (NKUA). The NKUA is the largest state institution of higher education in Greece and one of the largest universities in Europe, located near the centre of Athens and extends over 1300 acres (Figure 1).

Athens is the capital of Greece and is located in central Greece and has an estimated population of over 664,046 in the city (39 km²), or 3,090,508 in the metropolitan area (412 km²) according to 2011 census. According to Köppen climate classification, Athens has been classified as Csa (Interior Mediterranean, mild with dry and hot summer). On local scale, the Mediterranean climatic conditions are modified by urban structures and urban morphological data sets, which have to be taken into account for estimating the thermal ambient conditions. More specifically, these conditions are influenced by the radiation fluxes and thus the radiation budget, which in turns depend on the SVF at the observed location.

The well-known way of assessing the SVF in a single point of the examined area is capturing an 180 fisheye image of the surrounding area by using a camera with the

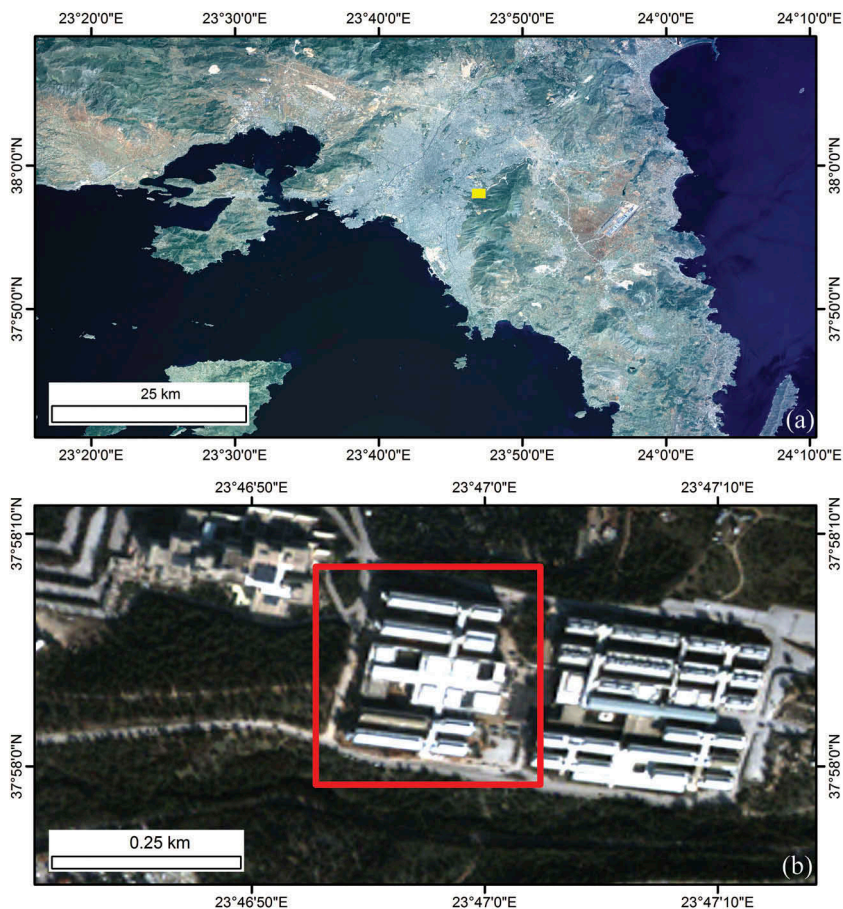


Figure 1. Location map of the study area (yellow square) regarding the urban metropolitan Athens city (a). Quickbird satellite image of the campus of National and Kapodistrian University of Athens (b) on which the inset red rectangle outlines the studied building complex.

fish-eye lens looking up to the sky, on a tripod at 1.1m height, where the gravity centre of the human body in Europe is considered (Mayer and Höpfe 1987; Nastos and Polychroni, 2016). In this study, fish-eye images have been captured using Sigma 4.5mm f/2.8 EX DC HSM circular fish-eye lens attached to a digital camera body (Canon 600D) facing upwards. Fish-eye lens has an angle of view of 180° in all directions, producing a perfectly circular image within the frame.

The SVF of an individual location is produced using the RayMan model (Matzarakis, Rutz, and Mayer 2010), which is developed to calculate short wave and long wave radiation fluxes affecting the human body. The model considers complex building structures and is suitable for the analysis of the effect of various planning scenarios in different micro to regional scales. The procedure of SVF estimation set out as follows: The captured fish-eye image is loaded into the 'Edit free sky view factor'-tool of the RayMan model. After that, the obstacles are digitized on screen and then the tool counts the sky pixels and relates them to the overall number of pixels in the image. Finally, a fish-eye image is produced which can also be used for deriving the sky view factor of the scenery modelled in the obstacle file.

However, if the continuous SVF of a whole area is the case, then SkyHelios model is used to calculate the SVF for a whole area. SkyHelios has been implemented in C# utilizing the 3D Graphics Library Mogre (MOGRE 2009). This implies that SkyHelios' main algorithms consist of creating a 3D-scene from raster or vector data, providing this scene to the graphics engine and then instructing the graphics engine how to perform meteorological/climatological modelling based on the scene. The graphics engine in turn will make the graphics processor (GPU) perform the requested modelling (see Matzarakis and Matuschek 2011, for a descriptive detail of SkyHelios). In SkyHelios, spatial information layers such as high resolution DEM of the studied area, can be loaded and by utilizing the computer's video card, fish-eye images are produced for each point throughout the studied area. The sky view factor at each point can be easily calculated from the produced fish-eye image by dividing the area of the image that is not covered by obstacles by the total image area. The result is a set of equally distributed points with an SVF-value generated for each point.

In this point, it is worth to note that the modelling of continuous SVF depends on the existence and on the accuracy of digital models of the urban structures of the area. The extremely high cost of acquiring lidar data in addition to the relatively lower spatial resolution comparing to SfM elevation data, as well as the dense building complex of the study area, led us to include the latter into the proposed methodology. A rotor-wing Remotely Piloted Airborne System (DJI Phantom 4 drone) was implemented during the field survey in order to collect high resolution natural colour images with its built-in camera bundled on a two-axis gimbal (see Table 1 for information). The platform is equipped with a GPS antenna which provides quite good precision for the horizontal and acceptable precision for the vertical axis which is also used for the alignment processing of the images captured during the survey (Fonstad et al. 2013).

The reliability of the modelled SVFs by applying SkyHelios model against observed SVFs by using fish-eye photographs (edited in RayMan model), is examined by utilizing the following statistical metrics: mean absolute error (MAE), mean bias error (MBE), root mean square error (RMSE), coefficient of determination (R^2), and index of agreement (IA) (Willmott 1982; Willmott et al. 1985; Comrie 1997; Walker et al. 1999; Kolehmainen et al.

Table 1. Main properties of the UAV survey and resulted datasets.

Attribute	Value
UAV platform	DJI Phantom 4
Sensor	FC3300 (focal length 3.61 mm)
Survey relative altitude (m)	90
Photo endlap (%)	90
Photo sidelap (%)	90
Total images	148
Image resolution	0.002 m
DEM resolution	0.09 m
Ortho-mosaic resolution	0.04 m

2001). A brief description of the statistical indices used in the quantitative analysis is presented in the following.

MAE is used to measure how modelled values are close to observed ones, and is given by formula (1):

$$\text{MAE} = \frac{1}{n} \sum_{i=1}^n |M_i - O_i|. \quad (1)$$

MBE is used to describe whether a model under (negative value) or over (positive value) estimates the observation, and is given by formula (2):

$$\text{MBE} = \frac{1}{n} \sum_{i=1}^n (M_i - O_i), \quad (2)$$

where n is the number of the data points, M_i and O_i represent modelled and observed values, respectively.

RMSE is a commonly used measure of the differences between the modelled and the observed values. The smaller the RMSE is the closer to the observations are the modelled values. RMSE is calculated according to formula (3):

$$\text{RMSE} = \left(\frac{1}{n} \sum_{i=1}^n (M_i - O_i)^2 \right)^{\frac{1}{2}}. \quad (3)$$

R^2 , which is a number between 0 and +1, measures the degree of association between two variables; in our case, the observed (O_i) and the modelled data (M_i). The coefficient of determination is computed according to formula (4):

$$R^2 = 1 - \frac{\sum_{i=1}^n (O_i - M_i)^2}{\sum_{i=1}^n (O_i - O_{i\text{mean}})^2}, \quad (4)$$

where $O_{i\text{mean}}$ represents the average of the observed values.

IA is a relative measure of error, and is calculated according to formula (5). This is a dimensionless measure that is limited within the range 0–1. IA equal to 0 (1) means no agreement (perfect agreement) between modelled and observed data.

$$IA = 1 - \frac{\sum_{i=1}^n (M_i - O_i)^2}{\sum_{i=1}^n (|M_i - O_{imean}| + |O_i - O_{imean}|)^2} \tag{5}$$

3. Results and discussion

In our study, two surveys were conducted for covering a total area of 2 km² around a complex building area at the NKUA campus. Each survey was scheduled at a flight elevation of 90 m above the take off point (located at the top of a 10 m high building) and lasted approximately 20 min. The applied procedure can be divided into three individual stages (Figure 2). Initially an image acquisition survey has to be designed, aiming to cover the study area with high resolution, overlapping, natural colour photographs. In order to obtain a satisfying overlap (70–90%) during the image acquisition, the flight height and the density of the images had to be taken under consideration, not to forget the battery usage limitations (see earlier). The percentage of overlapping is quite crucial as it had to be high enough for a successive interpretation and DEM construction without any artefacts, at a later stage. In such way, every single point is captured at least at two images from different angles and this satisfies the conditions for a successful completion of the DEM construction. Otherwise, points with false coordinates are displayed and also participate in the model solution, which produces errors in the final result. Additionally, topographic survey with

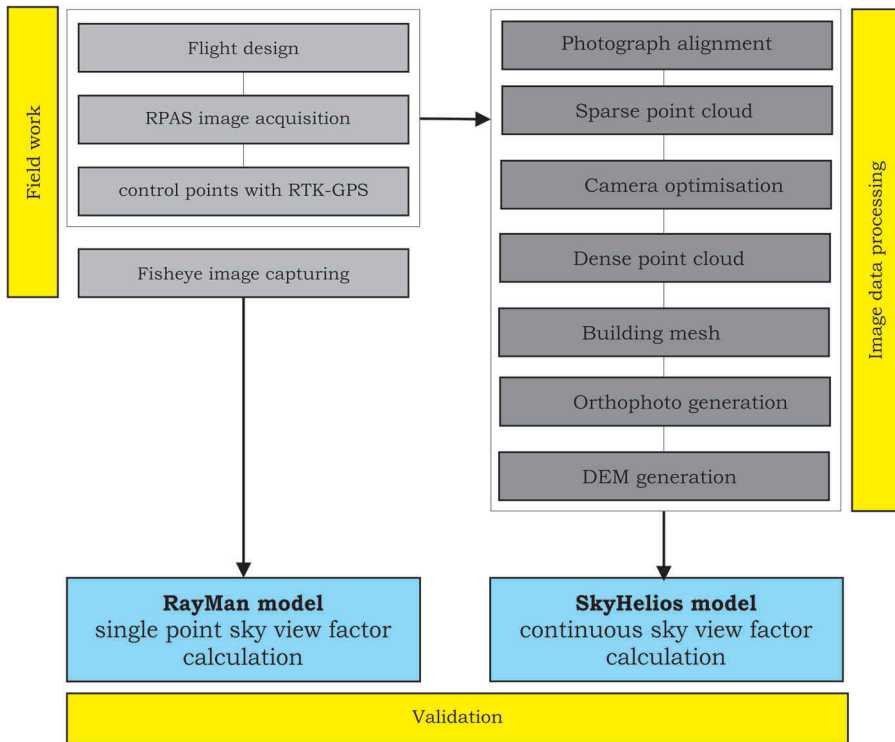


Figure 2. Flowchart of the processing steps followed for the calculation of the continuous SVF.

high precision equipment (real time kinematics GPS) was conducted for measuring 12 ground control points at locations of various elevations. These measurements were included in the model solution processing, for increasing the accuracy of the methodology (less than 1 cm), especially along the elevation axis.

The next stage consists of the main procedure of the image processing and interpretation, which can be described in a few steps. A total of 148 images (4000×3000 pixels each) was acquired with 90% overlapping and after aligning them a sparse 3D point cloud representing the most prominent features in the images was produced (Figure 3). Image processing followed the recommended procedure outlined by Agisoft (2016) which was slightly modified for reducing geometry errors and constructing a dense point cloud. The latter consisted of more than 30 million points covering the entire building complex and the surrounding area. The information for each point of them includes values of reflectance at the visible (BGR) spectra along with x , y , z coordinates, which were calculated after taking into account the positions of the camera when shooting at each point from different angles as well as the 12 measured control points (Westoby et al. 2012).

The procedure continued with meshing the original images as fine topographic details were available and the ultra-high resolution DEM can then be exported into various formats (Figure 4). Texturing was also applied to the resulted mesh in a next step and an ortho-image was generated for reference and comparative reasons. The combination of both the above products led to the three-dimensional representation of the studied building complex (Figure 5). It is worth to mention that the whole procedure of the computation was time and resource consuming and required the availability of large amount of RAM free (Mancini et al. 2013).

The final stage of the applied technique was based on the constructed DEM, which was downscaled to 0.5 m spatial resolution (Figure 4) and used as an input for the calculation of SVF at each pixel.

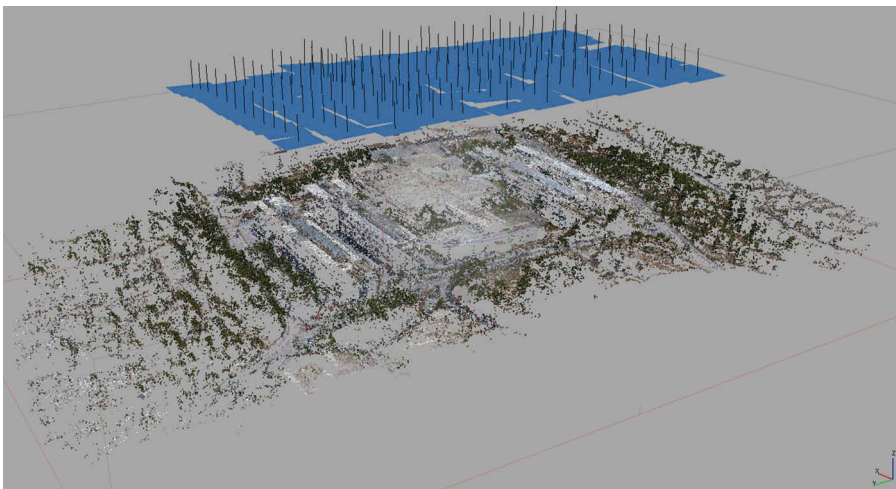


Figure 3. A sparse point cloud (only 1% of the total extracted points are displayed) of the University campus buildings is shown. The point cloud was extracted by using 148 overlapping images the location of which is also presented.

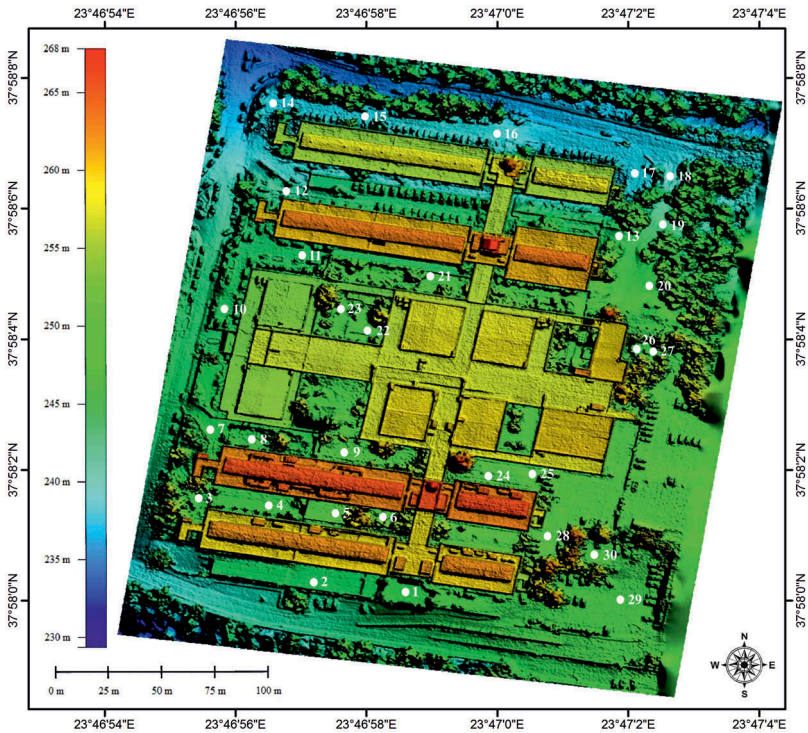


Figure 4. The shaded relief of the building complex at the study area is colour scaled by the use of the high resolution DEM which was one of the main products of the image interpretation procedure. Note that the colour scale is stretched between no more than 40 m. Numbers indicate the locations where fisheye images were captured to validate the modelled SVF.



Figure 5. The combination of the high resolution elevation data and the ortho-image led to the construction of the high detail 3D model of the complex building area in the campus of National and Kapodistrian University of Athens.

Based on the constructed high resolution DEM, the continuous SVF over the examined complex building area of the NKUA campus was estimated by using SkyHelios model (Figure 6). The SVF in building and green atriums ranges between 0.31 and 0.49

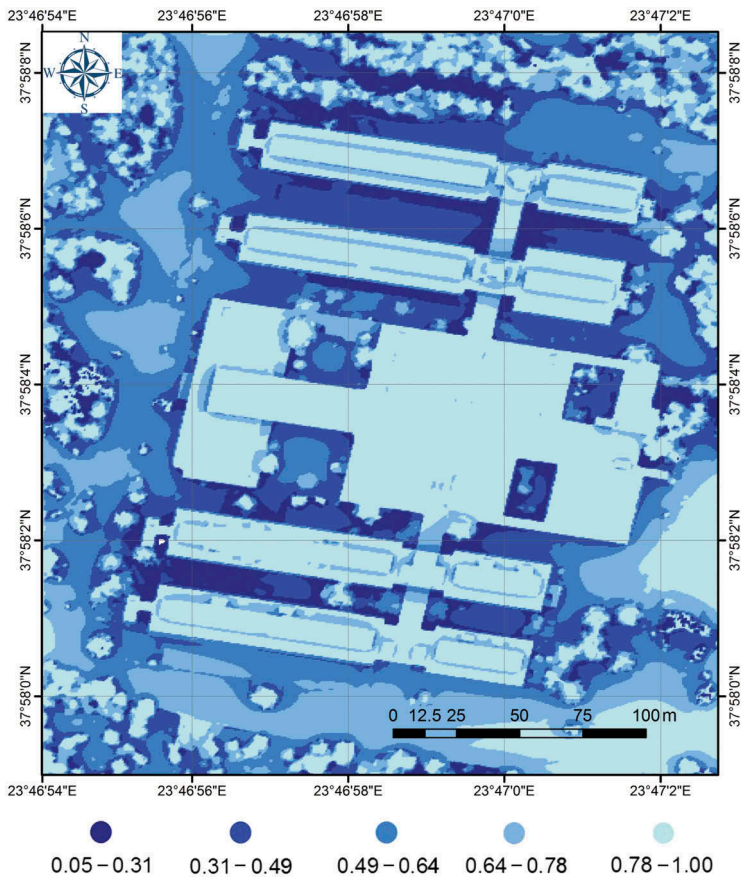


Figure 6. Spatial continuous SVF over the examined complex building area in the campus of National and Kapodistrian University of Athens.

and in some cases drops in the lower class (0.05–0.31). There are more open spaces with moderate SVF (0.49–0.64) against high SVF (0.64–0.78). The highest SVF appears obviously on the roofs of the buildings. In this point, it is worthy to note that the planting of trees (mainly pines) covering large area of NKUA campus, contributes in low SVF at green atriums, and thus in weakening of the incoming solar radiation, resulting in this way to comfortable thermal conditions especially within the summer months. The shading of trees and obstacles attenuate the incoming radiation, influencing in that way the human biometeorological conditions in outdoor spaces (Lin, Matzarakis, and Hwang 2010). Another issue is the orientation of the buildings in shading or not adjacent areas; meaning, either block (east–west orientation; e.g. locations 4 and 15 in Figure 4, with SVF of 0.290 and 0.0.305, respectively) or admit (north–south orientation; locations 10 and 17 in Figure 4, with SVF of 0.601 and 0.624, respectively) the incoming solar radiation to reach the ground. Oke (1988) suggested for mid-latitude cities with no overheating problems the acceptable range of height-to-width ($H:W$) ratio of the urban structure canyons would be 0.4–0.6, which corresponds to a range of SVF of 0.78–0.64.

To validate our findings by utilizing SkyHelios modelling, Figure 7 depicts SVF images acquired from fisheye images (true colours; edited by RayMan model) against the

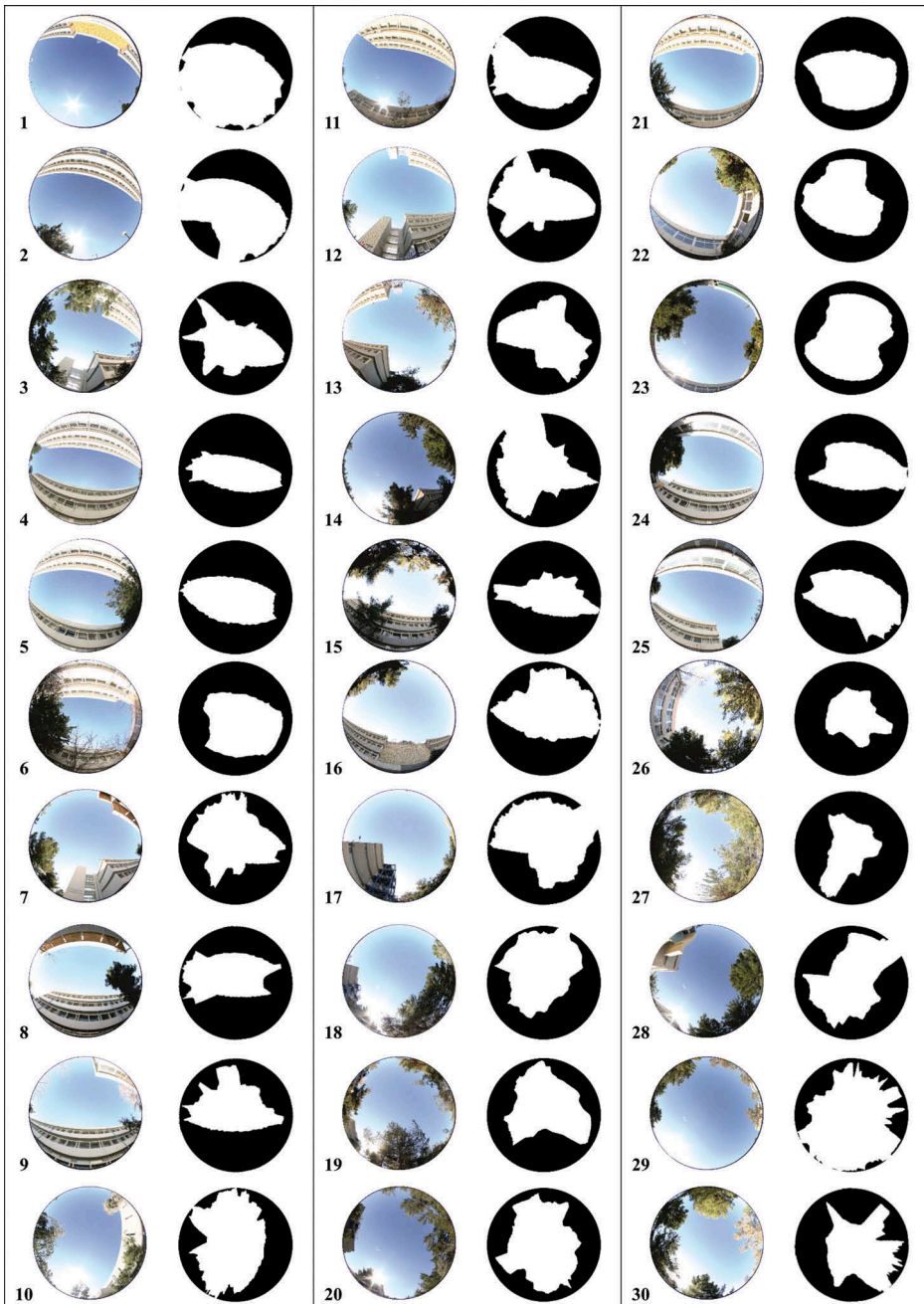


Figure 7. SVF acquired from fisheye images (true colour) against SVF from SkyHelios model using the ultra-high resolution DEM (black and white images), for 30 specific locations within the study area.

respective ones from SkyHelios model using the ultra-high resolution DEM (black and white images), for 30 specific locations (including building and green atriums, and open sky places) over the studied area (Figure 4). We performed quantitative analysis by calculating statistic metrics such as MAE, MBE, RMSE, R^2 , and IA, in order to verify our

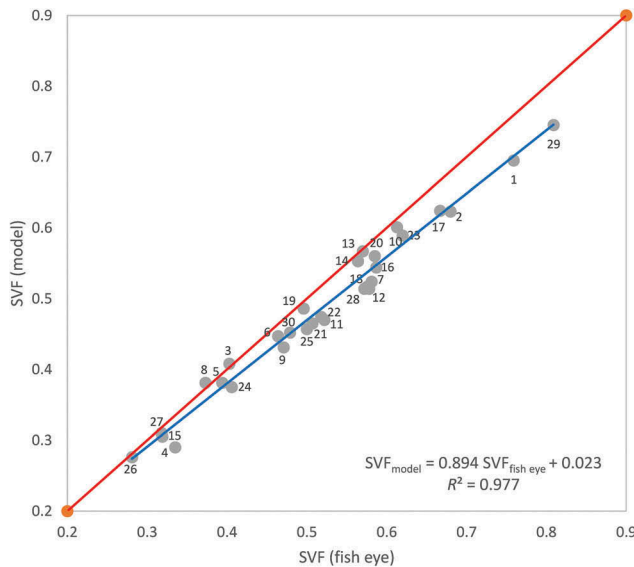


Figure 8. Scatter plot of modelled SVF by Sky Helios against observed SVF by fisheye images, along with the linear regression line (blue line) and the ideal line (red line).

findings. The small values of MAE (−0.032), BAE (0.033), and RMSE (0.039) indicate that the modelled SVFs are close to the observed SVFs. Further R^2 (0.977) confirms the high agreement between the examined SVF datasets, statistically significant at 0.01 level. Similarly, the index IA (0.974) confirms that the modelled SVF values are very reliable, which encourages the applied methodology to urban environmental research.

The scatter plot between the examined SVF pairs from the 30 specific locations, along with the linear regression fitting ($SVF_{\text{model}} = 0.894 SVF_{\text{fisheye}} + 0.023$) and the ideal line ($SVF_{\text{model}} = SVF_{\text{fisheye}}$) are depicted in Figure 8. The modelled SVF underestimates a little the observed SVF (MAE: −0.032), as the SVF values increases from green (site 26; $SVF = 0.276$) and building (site 8; $SVF = 0.381$) atriums towards open sky spaces (site 29; $SVF = 0.745$).

Although SVF is considered well correlated with surface temperature pattern at local scale (Barring, Mattsson, and Lindqvist 1985; Eliasson 1996), little evidence shows strong relationship between SVF and air temperature, due to complicated factors that modify air temperature variations. For a holistic assessment of the thermal comfort conditions in outdoor urban spaces other factors, apart from environmental configuration's characteristics and meteorological parameters, such as shading (Donovan and Butry 2009; Emmanuel, Rosenlund, and Johansson 2007; Hwang, Lin, and Matzarakis 2011; Nastos and Polychroni, 2016), and the existence of vegetation (Gomez, Gil, and Jabaloyes 2004; Potchter, Cohen, and Bitan 2006; Yu and Hien 2006) must be considered. Further, social customs (Heschong 1979) and the complexity of relation between human perception and thermal comfort in urban spaces (Nikolopoulou, Baker, and Steemers 2001) should be addressed.

4. Conclusions

In this study, a novel remote sensing approach was considered for establishing a new methodology to assess the continuous SVF for a complex building environment by using

the SfM technique, based on the interpretation of ultra-high resolution colour images acquired by UAVs. The accurate assessment of the continuous SVF over an urban complex area, is of utmost importance to quantify human thermal indices such as physiologically equivalent temperature (PET), universal thermal climate index (UTCI), and perceived temperature (PT), which are based on human energy balance.

The quantitative analysis, based on statistical metrics such as MAE, MBE, RMSE, R^2 , and IA, showed that the modelled SVF values are very reliable (statistically significant at $p = 0.01$ level) against observed SVF calculated from fisheye images captured at 30 specific locations of the NKUA campus. Further, the building and green atriums within NKUA campus, presenting small SVF values, could mitigate the heat stress in summer period. This is very encouraging for people to use these open spaces with comfortable environmental conditions.

Disclosure statement

No potential conflict of interest was reported by the authors.

ORCID

Emmanuel Vassilakis  <http://orcid.org/0000-0002-1175-3628>

References

- Agisoft. 2016. "Agisoft Photoscan User Manual: Professional Edition (v.1.2)." Accessed 23 July 2016. http://www.agisoft.com/pdf/photoscan-pro_1_2_en.pdf
- Bärring, L., J. Mattsson, and S. Lindqvist. 1985. "Canyon Geometry, Street Temperatures and Urban Heat Island in Malmö, Sweden." *Journal of Climatology* 5 (4): 433–444. doi:10.1002/joc.3370050410.
- Brown, M. J., S. Grimmond, and C. Ratti. 2001. "Comparison of Methodologies for Computing Sky View Factor in Urban Environments." International Society of Environmental Hydraulics Conference, Tempe, AZ, December 5–8.
- Charalampopoulos, I., I. Tsiros, A. Chronopoulou-Sereli, and A. Matzarakis. 2013. "Analysis of Thermal Bioclimate in Various Urban Configurations in Athens, Greece." *Urban Ecosystems* 16 (2): 217–233. doi:10.1007/s11252-012-0252-5.
- Comrie, A. C. 1997. "Comparing Neural Networks and Regression Models for Ozone Forecasting." *Journal of the Air & Waste Management Association* 47: 653–663. doi:10.1007/978-94-011-1122-5.
- Donovan, G., and D. Butry. 2009. "The Value of Shade: Estimating the Effect of Urban Trees on Summertime Electricity Use." *Energy and Buildings* 41 (6): 662–668. doi:10.1016/j.enbuild.2009.01.002.
- Dumas, E., and B. Baker. 2016. "UAV Research." *Metreorological Technology International*, April 20–24, pp. 20–24.
- Eliasson, I. 1996. "Urban Nocturnal Temperatures, Street Geometry and Land Use." *Atmospheric Environment* 30 (3): 379–392. doi:10.1016/1352-2310(95)00033-X.
- Emmanuel, R., H. Rosenlund, and E. Johansson. 2007. "Urban Shading—A Design Option for the Tropics? A Study in Colombo, Sri Lanka." *International Journal of Climatology* 27: 1995–2004. doi:10.1002/(ISSN)1097-0088.
- Fonstad, M., J. Dietrich, B. Courville, J. Jensen, and P. Carbonneau. 2013. "Topographic Structure from Motion: A New Development in Photogrammetric Measurement." *Earth Surface Processes and Landforms* 38 (4): 421–430. doi:10.1002/esp.3366.

- Gál, T., F. Lindberg, and J. Unger. 2009. "Computing Continuous Sky View Factors Using 3D Urban Raster and Vector Databases: Comparison and Application to Urban Climate." *Theoretical and Applied Climatology* 95: 111–123. doi:10.1007/s00704-007-0362-9.
- Gallay, M. 2012. "Section 2.1.4: Direct Acquisition of Data: Airborne Laser Scanning." In *Geomorphological Techniques (Online Edition)*, edited by S. J. Cook, L. E. Clarke, and J. M. Nield. London, UK: British Society for Geomorphology. ISSN: 2047-0371.
- Gomez, F., L. Gil, and J. Jabaloyes. 2004. "Experimental Investigation on the Thermal Comfort in the City: Relationship with the Green Areas, Interaction with the Urban Microclimate." *Building Environment* 39: 1077–1086. doi:10.1016/j.buildenv.2004.02.001.
- Grimmond, C. S. B., S. K. Potter, H. N. Zutter, and C. Souch. 2001. "Rapid Methods to Estimate Sky-View Factors Applied to Urban Areas." *International Journal of Climatology* 21 (7): 903–913. doi:10.1002/joc.659.
- Heschong, L. 1979. *Thermal Delight in Architecture*. Cambridge, MA: Massachusetts Institute of Technology Press.
- Holmer, B., U. Postgård, and M. Eriksson. 2001. "Sky View Factors in Forest Canopies Calculated with IDRISI." *Theoretical and Applied Climatology* 68 (1): 33–40. doi:10.1007/s007040170051.
- Hwang, R.-L., T.-P. Lin, and A. Matzarakis. 2011. "Seasonal Effects of Urban Street Shading on Long-Term Outdoor Thermal Comfort." *Building Environment* 46: 863–870. doi:10.1016/j.buildenv.2010.10.017.
- Jamei, E., Y. Jamei, P. Rajagopalan, D. R. Ossen, and S. Roushenas. 2015. "Effect of Built-Up Ratio on the Variation of Air Temperature in a Heritage City." *Sustainable Cities and Society* 14: 280–292. doi:10.1016/j.scs.2014.10.001.
- Javernick, L., J. Brasington, and B. Caruso. 2014. "Modeling the Topography of Shallow Braided Rivers Using Structure-from-Motion Photogrammetry." *Geomorphology* 213: 166–182. doi:10.1016/j.geomorph.2014.01.006.
- Johnson, K., E. Nissen, S. Saripalli, J. R. Arrowsmith, P. McGarey, K. Scharer, P. Williams, and K. Blisniuk. 2014. "Rapid Mapping of Ultrafine Fault Zone Topography with Structure from Motion." *Geosphere* 10 (5): 969–986. doi:10.1130/ges01017.1.
- Jones, P. D., D. H. Lister, and Q. Li. 2008. "Urbanization Effects in Large-Scale Temperature Records, with an Emphasis on China." *Journal of Geophysical Research: Atmospheres* 113 (D16). doi:10.1029/2008JD009916.
- Kolehmainen, M., H. Martikainen, and J. Ruuskanen. 2001. "Neural Networks and Periodic Components used in Air Quality Forecasting." *Atmospheric Environment* 35: 815–825. doi:10.1016/S1352-2310(00)00385-X.
- Kondratyev, K. Y., and C. Varotsos. 1995. "Atmospheric Greenhouse Effect in the Context of Global Climate Change." *Il Nuovo Cimento C* 18 (2): 123–151. doi:10.1007/BF02512015.
- Kraus, K., and N. Pfeifer. 1998. "Determination of Terrain Models in Wooded Areas with Airborne Laser Scanner Data." *ISPRS Journal of Photogrammetry and Remote Sensing* 53 (4): 193–203. doi:10.1016/S0924-2716(98)00009-4.
- Lin, T. P., K. T. Tsai, C. C. Liao, and Y. C. Huang. 2013. "Effects of Thermal Comfort and Adaptation on Park Attendance regarding Different Shading Levels and Activity Types." *Building and Environment* 59: 599–611. doi:10.1016/j.buildenv.2012.10.005.
- Lin, T.-P., A. Matzarakis, and R.-L. Hwang. 2010. "Shading Effect on Long-Term Outdoor Thermal Comfort." *Building and Environment* 45 (1): 213–221. doi:10.1016/j.buildenv.2009.06.002.
- Lindberg, F., and C. S. B. Grimmond. 2010. "Continuous Sky View Factor Maps from High Resolution Urban Digital Elevation Models." *Climate Research* 42: 177–183. doi:10.3354/cr00882.
- Lindberg, F., S. Thorsson, and B. Holmer. 2008. "SOLWEIG 1.0 - Modelling Spatial Variations of 3D Radiant Fluxes and Mean Radiant Temperature in Complex Urban Settings." *International Journal of Biometeorology* 52: 697–713. doi:10.1007/s00484-008-0162-7.
- Mancini, F., M. Dubbini, M. Gattelli, F. Stecchi, S. Fabbri, and G. Gabbianelli. 2013. "Using Unmanned Aerial Vehicles (UAV) for High-Resolution Reconstruction of Topography: The Structure from Motion Approach on Coastal Environments." *Remote Sensing* 5 (12): 6880. doi:10.3390/rs5126880.

- Mandanici, E., P. Conte, and V. Girelli. 2016. "Integration of Aerial Thermal Imagery, LiDAR Data and Ground Surveys for Surface Temperature Mapping in Urban Environments." *Remote Sensing* 8: 880. doi:[10.3390/rs8100880](https://doi.org/10.3390/rs8100880).
- Matzarakis, A., F. Rutz, and H. Mayer. 2010. "Modelling Radiation Fluxes in Simple and Complex Environments: Basics of the RayMan Model." *International Journal of Biometeorology* 54 (2): 131–139. doi:[10.1007/s00484-009-0261-0](https://doi.org/10.1007/s00484-009-0261-0).
- Matzarakis, A., and O. Matuschek. 2011. "Sky View Factor as a Parameter in Applied Climatology; Rapid Estimation by the SkyHelios Model." *Meteorologische Zeitschrift* 20 (1): 39–45. doi:[10.1127/0941-2948/2011/0499](https://doi.org/10.1127/0941-2948/2011/0499).
- Mayer, H., and P. R. Höppe. 1987. "Thermal Comfort of Man in Different Urban Environments." *Theoretical and Applied Climatology* 38: 43–49. doi: [10.1007/BF00866252](https://doi.org/10.1007/BF00866252).
- MOGRE. 2009. MOGRE. www.ogre3d.org/wiki/index.php/MOGRE
- Nastos, P. T., and I. D. Polychroni. 2016. "Modeling and in Situ Measurements of Biometeorological Conditions in Microenvironments within the Athens University Campus, Greece." *International Journal of Biometeorology* 60 (10): 1463–1479. doi: [10.1007/s00484-016-1137-8](https://doi.org/10.1007/s00484-016-1137-8).
- Nastos, P. T., and J. Kapsomenakis. 2015. "Regional Climate Model Simulations of Extreme Air Temperature in Greece. Abnormal or Common Records in the Future Climate?" *Atmospheric Research* 152: 43–60. doi:[10.1016/j.atmosres.2014.02.005](https://doi.org/10.1016/j.atmosres.2014.02.005).
- Nikolopoulou, M., N. Baker, and K. Steemers. 2001. "Thermal Comfort in Outdoor Urban Spaces: Understanding the Human Parameter." *Solar Energy* 70 (3): 227–235. doi:[10.1016/S0038-092X\(00\)00093-1](https://doi.org/10.1016/S0038-092X(00)00093-1).
- Nunez, M., I. Eliasson, and J. Lindgren. 2000. "Spatial Variations of Incoming Longwave Radiation in Göteborg, Sweden." *Theoretical and Applied Climatology* 67 (3): 181–192. doi:[10.1007/s007040070007](https://doi.org/10.1007/s007040070007).
- Oke, T. R. 1981. "Canyon Geometry and the Nocturnal Urban Heat Island: Comparison of Scale Model and Field Observations." *Journal of Climatology* 1 (3): 237–254. doi:[10.1002/joc.3370010304](https://doi.org/10.1002/joc.3370010304).
- Oke, T. R. 1988. "Street Design and Urban Canopy Layer Climate." *Energy and Buildings* 11 (1–3): 103–113. doi:[10.1016/0378-7788\(88\)90026-6](https://doi.org/10.1016/0378-7788(88)90026-6).
- Oke, T. R., G. T. Johnson, D. G. Steyn, and I. D. Watson. 1991. "Simulation of Surface Urban Heat Islands under 'Ideal' Conditions at Night Part 2: Diagnosis of Causation." *Boundary-Layer Meteorology* 56 (4): 339–358. doi:[10.1007/BF00119211](https://doi.org/10.1007/BF00119211).
- Potchter, O., P. Cohen, and A. Bitan. 2006. "Climatic Behavior of Various Urban Parks during Hot and Humid Summer in the Mediterranean City of Tel Aviv, Israel." *International Journal of Climatology* 26 (12): 1695–1711. doi:[10.1002/joc.1330](https://doi.org/10.1002/joc.1330).
- Shashua-Bar, L., and M. E. Hoffman. 2003. "Geometry and Orientation Aspects in Passive Cooling of Canyon Streets with Trees." *Energy and Buildings* 35 (1): 61–68. doi:[10.1016/S0378-7788\(02\)00080-4](https://doi.org/10.1016/S0378-7788(02)00080-4).
- Souza, L. C. L., D. S. Rodrigues, and J. F. Mendes. 2003. "A 3d-Gis Extension for Sky View Factors Assessment in Urban Environment." In Proceedings of the 8th International Conference on Computers in Urban Planning and Urban Management CUPUM'03, Sendai, Japan, May 27–30.
- Svensson, M., and I. Eliasson. 2002. "Diurnal Air Temperatures in Built-Up Areas in Relation to Urban Planning." *Landscape and Urban Planning* 61 (1): 37–54. doi:[10.1016/S0169-2046\(02\)00076-2](https://doi.org/10.1016/S0169-2046(02)00076-2).
- United Nations, Department of Economic and Social Affairs, Population Division. 2014. World Urbanization Prospects: The 2014 Revision, Highlights (ST/ESA/SER.A/352). Published by the United Nations, ISBN 978-92-1-151517-6
- Walker, S. E., L. H. Slørdal, C. Guerreiro, F. Gram, and K. E. Grønseth. 1999. "Air Pollution Exposure Monitoring and Estimation Part II. Model Evaluation And Population Exposure." *Journal of Environmental Monitoring* 1 (4): 321–326. doi:[10.1039/a902776i](https://doi.org/10.1039/a902776i).
- Watson, I. D., and G. T. Johnson. 1987. "Graphical Estimation of Sky View-Factors in Urban Environments." *Journal of Climatology* 7 (2): 193–197. doi:[10.1002/joc.3370070210](https://doi.org/10.1002/joc.3370070210).

- Westoby, M. J., J. Brasington, N. F. Glasser, M. J. Hambrey, and J. M. Reynolds. 2012. "Structure-From-Motion' Photogrammetry: A Low-Cost, Effective Tool for Geoscience Applications." *Geomorphology* 179: 300–314. doi:[10.1016/j.geomorph.2012.08.021](https://doi.org/10.1016/j.geomorph.2012.08.021).
- Willmott, C. J. 1982. "Some Comments on the Evaluation of Model Performance." *Bulletin of the American Meteorological Society* 63 (11): 1309–1313. doi:[10.1175/1520-0477\(1982\)063<309:scoteo><1309:scoteo>2.0.CO;21309:scoteo](https://doi.org/10.1175/1520-0477(1982)063<309:scoteo><1309:scoteo>2.0.CO;21309:scoteo).
- Willmott, C. J., S. G. Ackleson, R. E. Davis, J. J. Feddema, K. M. Klink, D. R. Legates, J. O'Donnell, and C. Rowe. 1985. "Statistics for the Evaluation and Comparison of Models." *Journal of Geophysical Research* 90 (C5): 8995–9005. doi: [10.1007/978-94-017-3048-8_23](https://doi.org/10.1007/978-94-017-3048-8_23).
- Wu, J., Y. Zhang, and Q. Meng. 2013. "Calculation Method of Sky View Factor Based on Rhino-Grasshopper Platform." 13th Conference of International Building Performance Simulation Association, Chambéry, France, August 26.
- Yu, C., and W. Hien. 2006. "Thermal Benefits of City Parks." *Energy and Buildings* 38 (2): 105–120. doi:[10.1016/j.enbuild.2005.04.003](https://doi.org/10.1016/j.enbuild.2005.04.003).
- Zakšek, K., K. Oštir, and Ž. Kokalj. 2011. "Sky-View Factor as a Relief Visualization Technique." *Remote Sensing* 3: 398. doi:[10.3390/rs3020398](https://doi.org/10.3390/rs3020398).